Low threshold InAs-based interband cascade lasers grown by MBE

*Kedong Zhang,[1, #] Yuzhe Lin,[2, #] Wanhua Zheng,[2,5 *] Rui Q. Yang,[3, *] Hong Lu,[1, 4 *] Yan-Feng Chen[1]*

[1] *National Laboratory of Solid State Microstructures & Department of Materials Science and Engineering, College of Engineering and Applied Sciences, Nanjing University, Nanjing, China*
[2] *Laboratory of Solid State Optoelectronics Information Technology, Institute of Semiconductors, Chinese Academy of Sciences, Beijing, China*
[3] *School of Electrical and Computer Engineering, University of Oklahoma, Norman, USA*
[4] *Jiangsu Key Laboratory of Artificial Functional Materials, Nanjing University, Nanjing 210093, China*
[5] *Center of Materials Science and Optoelectronics Engineering, University of Chinese Academy of Sciences, Beijing, China*

Corresponding author: hlu@nju.edu.cn, rui.q.yang@ou.edu, whzheng@semi.ac.cn

[#] *The authors contribute equally*

Mid-infrared interband cascade laser (ICL) structures aimed for emission at room temperature in the 4-5 µm wavelength region are grown by molecular beam epitaxy (MBE) on InAs substrates. High crystalline quality of the epitaxial structures has been confirmed by X-ray diffraction with thickness deviations less than 1% from the designs. Also, the average surface defect density is in the low ten to the fourth level. The broad-area (BA) devices made from the MBE-grown ICL wafers can lase in continuous wave (CW) mode in a wavelength range from 3.5 to 4.8 µm at temperatures up to 257 K, which is the highest reported for BA InAs-based ICLs at similar wavelengths. Their threshold current densities are low (e.g. 2.7 A/cm² at 80 K), indicating excellent material quality with a very low Shockley-Reed-Hall recombination. In pulsed mode, the lowest threshold current density is 252 A/cm² at 300 K, and the maximum operating temperature has reached 379 K. By comparisons in device performance among multiple MBE-grown ICL wafers, the importance of beam equivalent pressure stability and accurate control of layer thicknesses is demonstrated for the desirable performance.

Keywords: B3. Interband cascade laser, B3. Mid-infrared devices, A3. Molecular beam epitaxy, B2. Type-II quantum well

1. Introduction

Mid-infrared (IR) light sources have a wide range of applications, such as biological and medical diagnosis, environmental monitoring, industrial process control and free-space communications.[1-4] In the mid-IR spectral region, which is often called the molecular-fingerprint region, many molecules possess their fundamental vibration-rotational absorption lines. For the sensitive detection of those molecules with fast response, semiconductor mid-IR lasers are desirable. Currently, there are three major types of mid-IR semiconductor lasers: conventional type-I GaSb-based quantum well (QW) lasers,[5, 6] intraband quantum cascade lasers (QCLs),[7, 8] and interband cascade lasers (ICLs).[9-12] Although significant advances in traditional interband diode lasers have been achieved recently, especially beyond a wavelength of 3 µm, this conventional approach faces increasing difficulties for still longer wavelength operation because of higher threshold current densities with more QWs in the active region due to factors such as non-uniform carrier distribution and limited valence band offset. QCLs are based on intersubband transitions within the same band and can be tailored to cover the entire mid-IR spectrum without being restricted to the bandgap of available semiconductors.[7] Also, the cascade stages are connected in series within the same waveguide so that every injected electron can generate multiple photons to increase quantum efficiency and differential gain. However, due to inherent fast phonon scattering (on the order of ps or shorter), mid-IR QCLs typically have relatively high threshold current density (e.g., > 1 kA/cm² at 300 K) and high operating voltage (~10 V or higher), leading to a significant amount of input power density before reaching the threshold. ICLs, proposed originally in 1994,[9] retain the interband transitions for photon emission, in which the carrier lifetime is typically determined by Auger recombination and is on the order of

nanoseconds, and utilize type-II heterostructures to form a cascade configuration. Therefore, ICLs combine the advantages of QCLs and diode lasers, which can result in a low threshold current density and significantly reduced power consumptions, and have become important mid-infrared light sources.[10-12]

Based on interband transitions in type-II InAs/GaInSb QWs, ICLs can cover the important 3-5 μm wavelength region and beyond. [10-17] Excellent device performance at room temperature and above has been demonstrated from GaSb- and InAs-based ICLs covering wavelength range from 2.9 to beyond 6 μm.[10-12] Nevertheless, the ICL structure is relatively complicated and the growth of ICLs is much less mature compared to GaAs- and InP-based material growth technologies, which presented challenges to the development of high-performance ICLs. Additionally, ICL structures were initially grown and developed on GaSb substrates, while InAs-based ICLs were started much later and less explored. InAs-based ICLs use highly doped n-type InAs layers as the optical cladding instead of InAs/AlSb superlattices (SLs) that were commonly used in GaSb-based ICLs. Consequently, the growth of InAs-based ICLs is somewhat simplified with substantially reduced shutter movements. Furthermore, because the thermal conductivity of InAs is about 10 times of that of InAs/AlSb SL, InAs-based ICLs can have improved thermal dissipation. Hence, our initial effort was focused on the growth and development of InAs-based ICLs.

In this work, ICL structures were designed for lasing at room temperature in the 4-5 μm wavelength region with two waveguide configurations (as shown in Fig. 1). [18-20] The ICL structure in Fig. 1(a) has 12 cascade stages with heavily doped InAs (1×10^{19}/cm^3 by Si) cladding layers and two 1.2-μm-thick undoped InAs separate confinement layers (SCLs). The ICLs structure in Fig. 1(b) has 10 cascade stages with heavily doped InAs (1.5-1.8×10^{19}/cm^3 by Si) outer cladding layers, two 1-μm-thick InAs/AlSb SL intermediate cladding layers, and two 0.4-μm-thick undoped InAs SCLs. The waveguide configuration with hybrid cladding layers as shown in Fig. 1(b) is expected to enhance the confinement factor and reduce the optical loss, resulting in improved device performance compared to the waveguide configuration in Fig. 1(a). [20]

According to the designs, five ICL wafers A (N210331A), B (N210425A), C (N210427A), D (N210603A) and E (N210606A) were grown on InAs (100) substrates using a Veeco GENxplor molecular beam epitaxy (MBE) system. Wafer A is with the waveguide configuration of Fig. 1(a) and the rest wafers are with the waveguide including hybrid cladding layers as shown in Fig. 1(b). The crystalline quality of the ICL structures was studied by high-resolution X-ray diffraction (XRD). The broad-area (BA) devices made from these MBE-grown ICL wafers can lase in a wavelength range from 3.5 to 5.1 μm at various temperatures. In CW mode, the threshold current density is as low as 2.7 A/cm^2 at 80 K, indicating the excellent material quality with a very low Shockley-Reed-Hall recombination, and the maximum CW operating temperature (T_{maxcw}) of the BA devices is 257 K. In pulsed mode, the lowest threshold current density at 300 K is 252 A/cm^2, and the maximum pulsed operating temperature (T_{max}) is 379 K.

2. MBE growth, material characterization and device fabrication

The MBE (Veeco GENxplor) system is equipped with valved arsenic (As) and antimony (Sb) crackers. All the effusion cells for the group III elements are dual filament SUMO cells. Reflection high energy electron diffraction (RHEED) was used for in-situ monitoring of the as-grown sample surface. All the InAs substrates were thermally heated under an As$_2$ beam equivalent pressure of 1×10^{-5} torr to remove the native oxides for about 30 min at 510°C, during which a clear surface reconstruction transition from 3× to 2× [21] can be seen. Then the substrates were cooled to 450 °C for the growth of the InAs buffer. The growth rate of InAs is 0.42 ML/s. The As/In ratio is controlled between 8~12 to achieve a slight As$_2$ overpressure as determined by the As-rich (2×4) surface.[22] The layered ICL structures are shown in Fig. 1(a) and 1(b). The whole structure was grown at 400°C as a compromise between the optimal growth windows for the thick InAs layers and the InAs/AlSb/Ga(In)Sb layers in the cascade regions. The growth temperature was calibrated using the surface reconstruction transition from (1×3) to (2×5) on a GaSb surface. Each cascade stage was composed of a "W"-shape QW active region made of InAs/Ga$_{0.7}$In$_{0.3}$Sb/InAs or

InAs/Ga$_{0.65}$In$_{0.35}$Sb/InAs, an n-type electron injector made of InAs/AlSb multiple QWs and a hole injector made of GaSb/AlSb QWs. Some of the InAs QWs in the electron injector were heavily n-doped using silicon to achieve the carrier rebalancing [15] with the hole concentration. The AlAs interfacial layers were inserted for strain balance. The thickness of the cascade region in each wafer was ~40 nm, which was confirmed by high-resolution XRD (Bruker D8 Advanced). The targeted thickness of InAs is 2.5 nm in the InAs/AlSb SL with a period of 4.8 nm. The Cu Kα1 line is used in the high-resolution XRD and the wavelength is 0.15406 nm.

The crystalline quality of the ICL structures was characterized using XRD and the corresponding spectra of the two different waveguide configurations are shown in Fig. 1(c) and 1(d). The satellite peaks due to the periodic structures can be seen around the InAs (004) peak for ICL-A in Fig. 1(c), indicating the sharp interfaces and high crystalline quality. The lattice mismatch between the cascade region and the InAs substrate is only -0.02%, and the deviation between the actual thickness and the designed value is 0.95%, indicating the excellent growth control by MBE. The surface smoothness is confirmed by atomic force microscope showing a root-mean-square roughness of 1.54 nm. For the wafers using the waveguide in Fig. 1(b), two 200-period InAs/AlSb SLs were added on both sides of the cascade region. As is seen in Fig. 1(d), additional set of satellite peaks (labeled in blue) with stronger intensity and larger spacing appeared for ICL-B compared to that in Fig. 1(c), which are caused by the periodicity of the InAs/AlSb SLs. The lattice mismatch between the InAs/AlSb superlattices and the InAs substrate is +0.26%. For the cascade region, it is fully lattice-matched with the substrate through further optimization of the AlAs interfacial thickness. Also, the typical full width of half maximum of the cascade satellite peaks is 45 arcsec, implying that the crystalline quality is not affected by the insertion of InAs/AlSb superlattices. The thickness deviation for the cascade region and InAs/AlSb superlattices is 0.6% and 1.33%, respectively. The uniformity of the wafers was examined by XRD spectra at different locations of a wafer. For example, as shown in Fig. 1(d), the XRD spectra obtained from the center (black) and near the edge (red) of a 2" wafer matched very well, indicating excellent uniformity of the grown material. The surface smoothness is greatly improved after further optimization of the growth conditions. As shown in Fig. 2(a), a root-mean-square (RSM) roughness of 167 pm is obtained on ICL-B. Also, the defect density is critical in the laser fabrication and performance. With careful control of the surface treatment and growth conditions, a defect density in the low ten to the fourth level has been achieved for all the five wafers. The defect density and distribution were studied using optical microscope. For example, the defect density of ICL-B, is in the range of 7.0×10^3-1.3×10^4 /cm^2 from different areas of the 2" wafer. Two different types of defects are shown in Fig. 2(b). One is the typical oval defect formed from the interface between the substrate and the epitaxial layer, the size of which is compatible to the thickness of the epitaxial layer, and they are marked by the red circles. The other smaller point defects are marked by the white circles.

After the epitaxial growth of the ICL structures, BA (150- and 100-μm-wide) mesa stripe lasers were fabricated by wet chemical etching and cleaved into cavities of 1.5 mm without facet coating. The lasers were mounted epi-layer side up on copper heat sinks for testing in CW and pulsed modes. In pulsed measurements, the pulsed current source with 1-μs-wide pulses at a repetition rate of 5 kHz (0.5% duty cycle) was applied to reduce the effect of Joule heating.

3. Device performance and discussion

BA devices made from all five wafers were able to lase at temperatures above 200 K in CW mode and above 300 K in pulsed mode. As shown in Fig. 3, the lasing wavelengths of the representative BA devices for all the ICLs were from 3.5 to 4.8 μm in CW mode operation and reached up to 5.1 μm at high temperatures in pulsed mode. For example, a device from wafer ICL-A had its lasing wavelength red shifted from 3.85 to 4.23 μm in CW mode as the temperature increased from 80 to 219 K, and to 4.6 μm in pulsed mode at 331 K. Compared to wafer A, devices made from wafers B, C, D and E could lase in CW mode at substantially higher temperatures with reduced threshold current densities and lowered threshold voltage as shown in Fig. 3 and Fig. 4. The maximum CW operation temperature was 257 K for a BA device made from wafer B with a lasing wavelength near 4.77 μm as shown in Fig. 4(a), which is the highest

reported for BA InAs-based ICLs at similar wavelengths. This validated the benefit of the enhanced optical confinement and reduced internal loss with the hybrid cladding layers.[11, 20] All the lasers had a threshold current density of a few A/cm^2 at 80 K. For instance, two 150-µm-wide devices made from wafer B had a threshold current density as low as 2.7 A/cm^2 at 80 K, which is among the best reported for mid-infrared semiconductor lasers[12, 20], suggesting excellent material quality with a low Shockley-Reed-Hall recombination. Characteristics of the BA devices are summarized in Fig. 4.

In pulsed mode, devices made from all the wafers could operate well above room temperature as summarized in Table I. The lasers with the hybrid cladding layers exhibited lower threshold current densities and voltages, and could operate at higher temperatures compared to devices from wafer A. A device from wafer C operated up to 379 K with a lasing wavelength near 4.9 µm, which is the highest reported operating temperature for ICLs at similar wavelengths. Also, at 300 K, the threshold current density is 252 A/cm^2 for device ICL-C, significantly lower than 533A/cm^2 for ICL-A. These results again prove the advantages of the hybrid cladding layers for reducing internal optical loss and improving optical confinement. For all the ICLs, the voltage efficiency as shown in Fig. 4(b) is higher than 70% in a wide temperature range. The highest voltage efficiency at 300 K is about 80% for ICL-C and ICL-D, which is better than the GaSb-based ICLs at similar lasing wavelengths, indicating more effective and smoother carrier transport in these InAs-based ICLs. It should be noted that devices from wafers D and E performed somewhat below what was expected compared to wafers B and C. This is because wafers D and E were grown near the end of this growth campaign and beam equivalent pressures started to drift so that the actual ICL layers were thinner than the designed values and consequently the lasing wavelengths became shorter than the targeted ones, resulting in higher threshold current densities than that in devices made from wafers B and C. Despite some deviations from the designs in the actual growths, devices from wafers D and E could still operate above room temperature with reasonable threshold current densities (*e.g.*, < 500 A/cm^2 at 300 K) in pulsed modes, which reflect reasonable durability of ICLs against structural variations [23]. On the other hand, the fact of the significantly higher threshold current density and lower maximum operating temperature for devices made from wafer E compared to devices made from wafers B and C suggests the importance for actual MBE growth to maintain stable beam equivalent pressures and achieve accurate agreement with the design.

To examine the passivation of device fabrication, a piece of wafer E was later processed into narrow ridge waveguide devices without a thick Au layer and cleaved into a 1.5 mm-long cavity without facet coating. The devices were mounted epi-side up on a copper heat sink. Several 15-µm-wide devices were able to lase in CW mode at temperatures up to 271 K near 4.3 µm (Fig. 5). Their representative current-voltage-light characteristics are shown in Fig. 5. In CW operation at temperatures from 80 to 200 K, the threshold current density of the narrow ridge device is nearly identical to that of the BA devices made from the same wafer, indicating excellent passivation on side-walls of these narrow ridge devices. This is also reflected by the sharp turn-on in the current-voltage characteristics as shown in Fig. 5. The thermal management was not optimized as indicated by the maximum threshold current density of ~600 A/cm^2 that the device could sustain, which limited the CW operation to 271 K. Hence, with substantially reduced threshold current densities, it is expected that the narrow ridge devices made from wafers B and C will operate in CW at room temperature and above when thermal management is improved with means such as a thick electroplated Au layer or epi-side down mounting.

4. Conclusions

High quality mid-IR ICL structures have been grown by MBE on InAs substrates and made into devices covering lasing wavelength from 3.5 to 5.1 µm. The fabricated ICLs have exhibited excellent device performance characteristics in terms of low threshold current densities (e.g., 2.7 A/cm^2 at 80 K and 252 A/cm^2 at 300 K) and maximum operating temperatures (e.g. 257 K and 379 K for the BA devices in CW and pulsed modes, respectively). By comparing the device performance of ICLs with two different waveguide configurations, the advantages of ICLs with the hybrid cladding layers were confirmed. With a series of consecutive growths of ICLs by MBE during one growth campaign, we demonstrated the

reasonable durability of ICLs against structural variations in MBE growth and the importance of stable beam equivalent pressures and accurate control for high device performance.

References

[1] R. D. Hudson, *Infrared System Engineering*, Wiley, New York (1969).
[2] D. S. Bomse, D. C. Hovde, D. B. Oh, J. A. Silver, A. C. Stanton, *Proc. SPIE* 1681 (1992) 138.
[3] P. Werle, K. Maurer, R. Kormann, R. Mücke, F. D'Amato, T. Lancia, A. Popov, *Spectrochim. Acta A Mol. Biomol. Spectrosc.* 58 (2002) 2361.
[4] F. K. Tittel, G. Wysocki, A. A Kosterev, Y. A. Bakhirkin, *Mid-Infrared Coherent Sources and Applications*, M. Ebrahim-Zadeh and I.T. Sorokina (eds.), Springer (2008) 467–493.
[5] K. Vizbaras, A. Vizbaras, A. Andrejew, C. Grasse, S. Sprengel and M.-C. Amann, "Room-temperature type-I GaSb-based lasers in the 3.0 – 3.7 μm wavelength range", Proc. SPIE **8277**, 82771B (2012).
[6] G. Belenky, L. Shterengas, M.V. Kisin, and T, Hosoda, "Gallium antimonide (GaSb)-based type-I quantum well diode lasers: recent development and prospects", Chap. 11, in *Semiconductor Lasers: Fundamentals and Applications*, edited by A. Baranov and E. Tournie (Woodhead Publishing Limited, Cambridge, UK, 2013).
[7] J. Faist, F. Capasso, D.L. Sivco, C. Sirtori, A.L. Hutchinson, A.Y. Cho, *Science* 264 (1994) 553–556.
[8] M. S. Vitiello, G. Scalari, B. Williams, N. P. De, *Opt. Express* 23 (2015) 5167.
[9] R. Q. Yang, *Superlattices Microstruct.* 17 (1995) 77.
[10] J. Koeth, R. Weih, J. Scheuermann, M. Fischer, A. Schade, M. Kamp, S. Hofling, *Proc. SPIE* 10403 (2017) 1040308.
[11] R. Q. Yang, L. Li, W. Huang, S. S. Rassel, J. A. Gupta, A. Bezinger, X. Wu, S.G. Razavipour, G. Aers, *IEEE J. Selected Topics Quantum Electronics.* 25 (2019) 1200108.
[12] J. R. Meyer, W. W. Bewley, C. L. Canedy, C. S. Kim, M. Kim, C. D. Merritt, I. Vurgaftman, *Photonics*. 7 (2020) 75.
[13] L. Li, H. Ye, Y. Jiang, R. Q. Yang, J. C. Keay, T. D. Mishima, M. B. Santos, M. B. Johnson, *J. Cryst. Growth* 425 (2015) 369–372.
[14] R. Q. Yang, L. Li, L. Zhao, Y. Jiang, Z. Tian, H. Ye, R. T. Hinkey, C. Niu, T. D. Mishima, M. B. Santos, *Proc. SPIE* 8640 (2013) 86400Q.
[15] I. Vurgaftman, W. W. Bewley, C. L. Canedy, C. S. Kim, M. Kim, C. D. Merritt, J. Abell, J. R. Lindle, J. R. Meyer, *Nature Commun.* 2 (2011) 585.
[16] M. Edlinger, R. Weih, J. Scheuermann, L. Naehle, M. Fischer, J. Koeth, M. Kamp, S. Hoefling, *Appl. Phys. Lett.* 109 (2016) 201109.
[17] M. Kim, W. W. Bewley, C. L. Canedy, C. S. Kim, J. R. Meyer, Opt. Express 23 (2015) 9664.
[18] Z. Tian, L. Li, Y. Hao, R. Q. Yang, T. D. Mishima, M. B. Santos, and M. B. Johnson, "InAs-based interband cascade lasers with emission wavelength at 10.4 μm", Electronics Lett. **48**, 113 (2012).
[19] Z. Tian, Y. Jiang, L. Li, R. T. Hinkey, Z. Yin, R. Q. Yang, T. D. Mishima, M. B. Santos, and M. B. Johnson, *IEEE J. Quantum Electron.* 48 (2012) 915.
[20] L. Li, Y. Jiang, H. Ye, R. Q. Yang, T. D. Mishima, M. B. Santos, M. B. Johnson, *Appl. Phys. Lett.* 106 (2015) 45.
[21] R. Contreras-Guerrero, S. Wang, M. Edirisooriya, W. Priyantha, J. S. Rojas-Ramirez, K. Bhuwalka, G. Doornbos, M.Holland, R. Oxland, G. Vellianitis, M. VanDal, B. Duriez, M. Passlack, C. H. Diaz, R. Droopad, *J. Cryst. Growth* 378 (2013) 117-120.
[22] H. Ye, L. Li, R.T. Hinkey, R.Q. Yang, T.D. Mishima, J.C. Keay, M.B. Santos, M.B. Johnson, *J. Vac. Sci. Technol. B* 31 (2013) 03C135.
[23] Y. Lin, J. A. Massengale, W. Huang, R. Q. Yang, T. D. Mishima, M. B. Santos, "Examination of the Durability of Interband Cascade Lasers Against Structural Variations", J. Infrared & Millimeter Waves. **39** (2), 137-141 (2020).
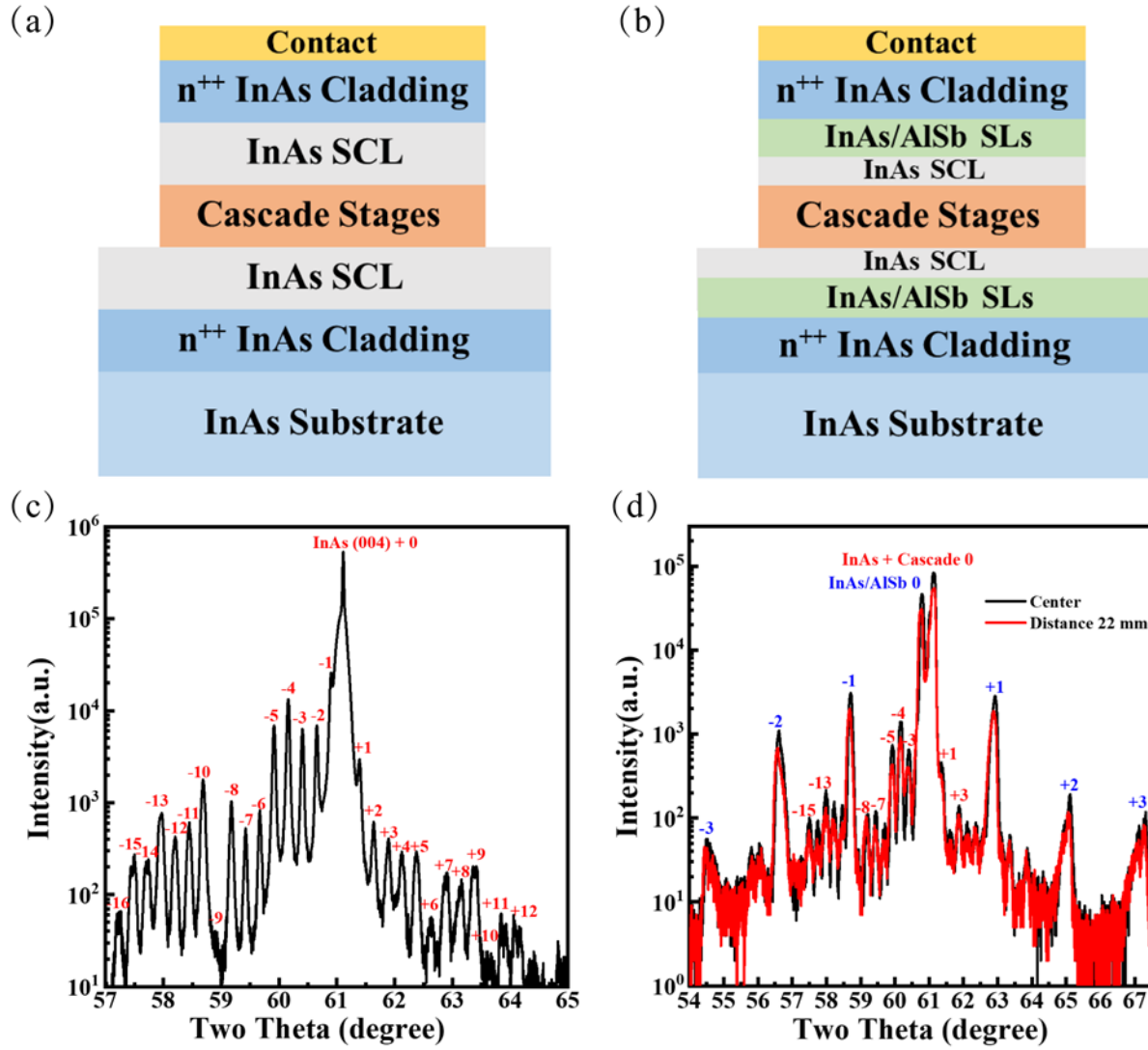
Fig. 1. The schematic diagram of two ICL structures (a), (b) and the corresponding XRD spectra (c), (d), respectively.
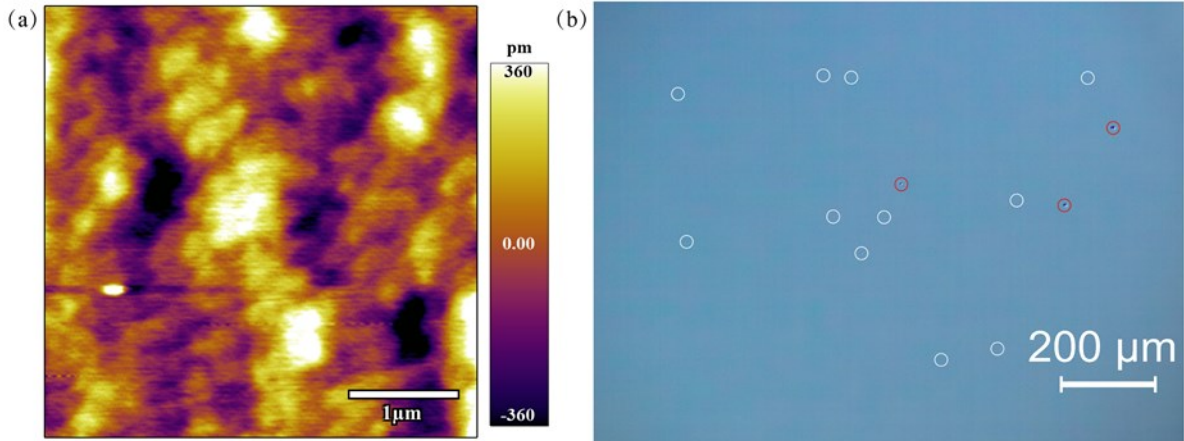

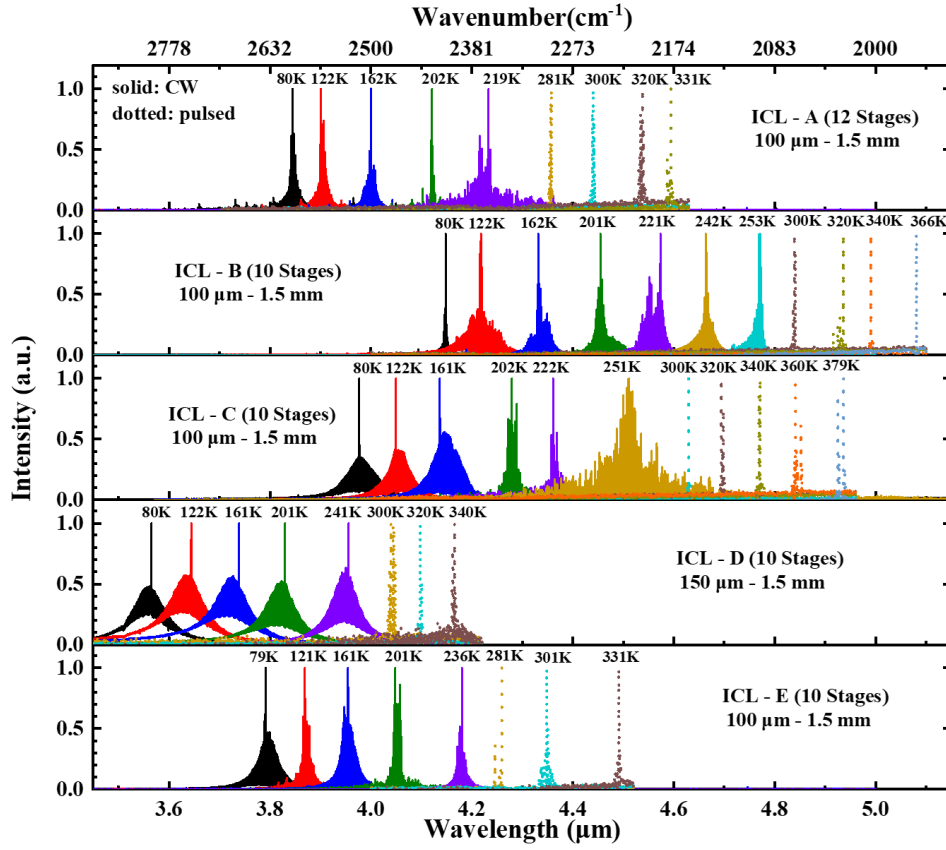**Fig. 2.** The AFM image (a) and Nomarski image (b) of ICL-B.

Fig. 3. The lasing spectra at various temperatures near the threshold of the lasers in CW and pulsed modes from ICL-A, and ICL-B, ICL-C, ICL-D, ICL-E.
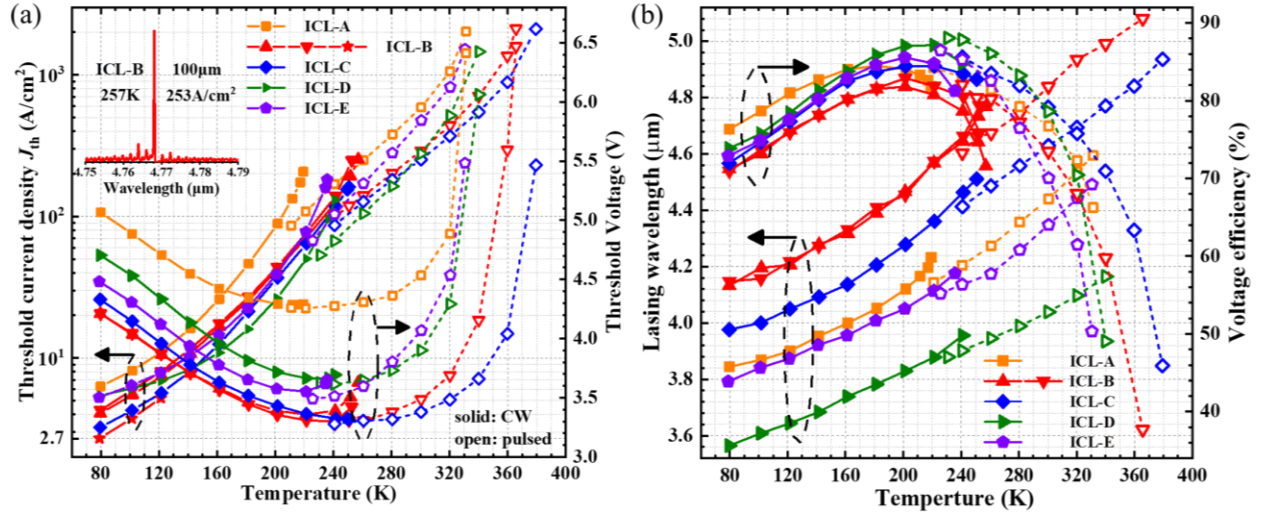

Fig. 4. (a) Temperature dependent threshold current density and voltage of the lasers in CW and pulsed modes. (b) Lasing wavelength and voltage efficiency vs. temperature.
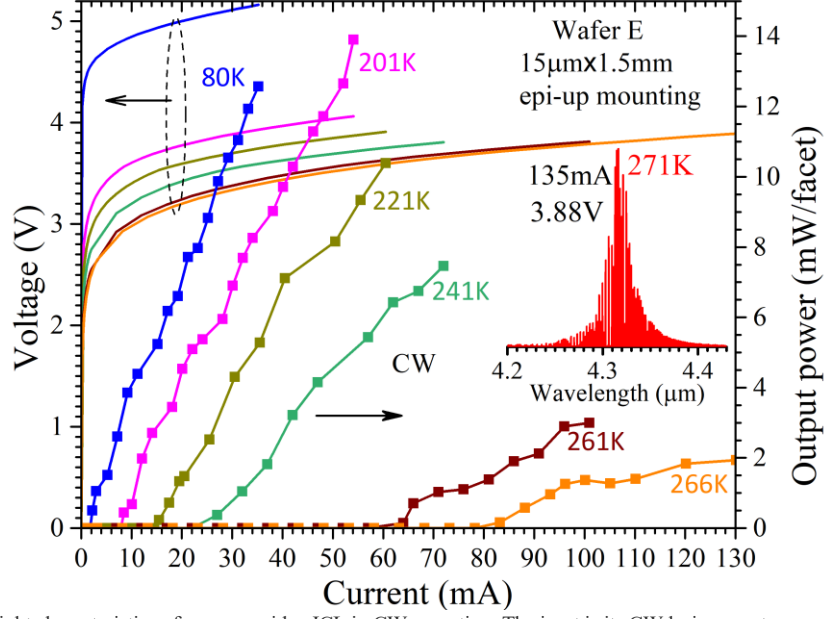
Fig. 5. Current-voltage-light characteristics of a narrow ridge ICL in CW operation. The inset is its CW lasing spectrum near threshold at 271 K.

TABLE I. CW and pulsed performance features of BA ICL devices

Wafer	cladding	CW J_{th} at 80 K (A/cm^2)	CW J_{th} (A/cm^2) at T_{maxcw} (K)	Pulsed J_{th} at 300K (A/cm^2)	Pulsed J_{th} (kA/cm^2) at T_{max} (K)	λ at 300K (μm)
ICL-A	n^+-InAs	6.30	207@219	533	2.03@331	4.46
ICL-B	hybrid	2.70	253@257	269	1.88@367	4.84
ICL-C	hybrid	3.23	161@251	252	2.11@379	4.63
ICL-D	hybrid	3.93	162@248	278	1.46@340	4.04
ICL-E	hybrid	5.10	180@236	477	1.52@331	4.35